Flow lines and mixing within drops in microcapillaries

François Blanchette
School of Natural Sciences, University of California–Merced, 5200 N. Lake Road, Merced, California 95343, USA
(Received 15 May 2009; published 28 December 2009)

We present a theoretical and numerical investigation of streamlines and mixing within drops flowing in capillaries. We first study theoretically the limit case of purely viscous flow around a drop of negligible radius, and find that, owing to geometrical constraints, recirculating regions are always present at the front and back of such drops. Using two-dimensional simulations, we visualize streamlines for larger drops, showing that the extent of these recirculating torii increases with drop size and decreases with Reynolds number. We study the mixing within drops as they are subjected to time-dependent shear, thus modeling a sinusoidal channel, and find that while cross-stream mixing is efficient, streamwise mixing is hindered by the front and back recirculating regions.

DOI: 10.1103/PhysRevE.80.066316 PACS number(s): 47.61.Ne

I. INTRODUCTION

The recent development of networks of pipes small enough to fit on a chip have opened a new realm of possibilities for microscale biological and chemical experiments. An extensive literature is devoted to this field, headed by the *Laboratory on a Chip* journal. In particular, micron-size droplets can be used as tiny insulated reactors in which reactions involving only picoliters of reagents may be observed [1,2]. Of paramount importance in the efficiency of these devices is the capability to quickly achieve mixing within the drop. Several mechanisms have been suggested to achieve such mixing. Active mechanisms such as pressure, dielectrophoretic, or electrokinetic disturbances (see [3] for a review), and thermocapillary effects [4] impose a time-varying flow through some external forcing. Passive mechanisms, on the other hand, rely on fixed designs, typically in the geometry of the capillary [3]. One of the simplest design consists of forcing the drops through planar sinuous pipes [5]. It was observed that mixing within drops could then take place on a scale of milliseconds.

While the experimental realization of drops flowing in sinuous channels has been mastered a few years ago, a precise description of the resulting flow has only been recently developed. Of particular interest is the flow pattern in and around the drop, and the resulting mixing within the drop. Direct observations have been attempted [6,7], but the small size and relatively high velocity of the drops have limited the scope of achievable results. Numerical simulations have been arguably more successful, beginning with a simplified model [8–10], and progressively obtaining a more accurate description of the system [11–13]. One significant finding of some of these studies [7,11,12] is the existence of a so-called dead region in the front and back of such drops, where the toroidal circulation taking place in the rest of the drop did not extend. Mixing was consequently less efficient in those regions. The origin of these relatively stagnant regions and the conditions, under which they occur have yet to be explained, and are the subject of the present study. We also study how such regions affect mixing within drops.

We present in this paper a detailed description of the flow in and around drops in capillaries that are displaced by a pressure gradient. We set the governing equations in Sec. II before describing an analytical solution to the idealized problem of a spherical drop of negligible radius traveling in a capillary in purely viscous flow, focusing on the flow within the drop in Sec. III. This analysis provides us with insight as to the origin of the counter-rotating torii at the drop's extremities. We then present in Sec. IV numerical simulations that show streamlines in and around larger drops, including inertial and deformation effects. In Sec. V, we use time-dependent shear to model a sinuous channel and study the mixing within the drop, both streamwise and crosswise. The influence of the drop radius, Reynolds number, Capillary number, and viscosity ratio is investigated.

II. SETUP AND GOVERNING EQUATIONS

We consider a drop, or drops, in a capillary tube. We refer to the outer fluid as the carrier fluid, and to the inner fluid as the drop fluid, including when that fluid is air. Both fluids are assumed to be Newtonian and incompressible. We consider immiscible fluids that are separated by a fluid interface subject to a constant surface tension σ. The Navier-Stokes equations therefore govern the velocity, $\vec{u}$, and pressure, P, of both fluids,

$$\nabla \cdot \vec{u} = 0, \tag{1}$$

$$\rho\left(\frac{\partial \vec{u}}{\partial t} + \vec{u} \cdot \nabla \vec{u}\right) = -\nabla P + \nabla \cdot (\mu \nabla \vec{u}) + \rho \vec{g}, \tag{2}$$

where $\vec{g}$ is the gravity vector, μ the viscosity, and ρ the density of the fluid.

At the interface, the normal stress jump is the product of twice the mean surface curvature, κ_m, and the surface tension σ, and in the absence of surface tension gradients, the tangential stresses are matched. On the interface, we then have

$$\hat{\tau} \cdot [\mu_d\{\nabla \vec{u}_d + (\nabla \vec{u}_d)^T\} - \{\mu_c \nabla \vec{u}_c + (\nabla \vec{u}_c)^T\}] \cdot \hat{n} = 0 \tag{3}$$

$$\hat{n} \cdot [\{-P_d \bar{\bar{I}} + \mu_d[\nabla \vec{u}_d + (\nabla \vec{u}_d)^T]\} - \{-P_c \bar{\bar{I}} + \mu_c[\nabla \vec{u}_c + (\nabla \vec{u}_c)^T]\}] \cdot \hat{n} = -2\sigma\kappa_m, \tag{4}$$

where the indices "d" and "c" refer to the drop and carrier

fluids, respectively, and the vectors $\vec{n}$ and $\vec{\tau}$ are, respectively, normal and tangent to the interface. While the pressure is typically discontinuous across the interface, the velocities are matched: $\vec{u}_d = \vec{u}_c$.

As is commonly the case in experiments [2], we focus on drops that do not wet the capillary, so that no contact lines need to be traced. No-slip conditions are imposed at the capillary walls, $\vec{u}_c = 0$. The drops are forced into motion by a constant pressure gradient imposed in a direction parallel to the tube's axis. Both fluids are initially at rest, but they quickly reach a steady state where the drops travel at a constant velocity.

We introduce a concentration function C, which describes the volume fraction of carrier liquid at any given location and is $C=0$ in the drop fluid and $C=1$ in the carrier fluid. We may then define a density and viscosity that are valid everywhere in the domain considered: $\rho = \rho_c(1 + \frac{\rho_d - \rho_c}{\rho_c} C)$ and $\mu = \mu_c(1 + \frac{\mu_d - \mu_c}{\mu_c} C)$. To facilitate our analysis, we recast equations (1) and (2) in nondimensional terms. We use the tube diameter, d, as a typical lengthscale, the carrier fluid density, ρ_c, as a density scale, and the centerline velocity in the absence of a drop, u_m, as a velocity scale, leaving us with

$$\nabla \cdot \vec{u} = 0, \tag{5}$$

$$\rho\left(\frac{\partial \vec{u}}{\partial t} + \vec{u} \cdot \nabla \vec{u}\right) = -\nabla P + \nabla \cdot \left[\frac{1 + C(\lambda - 1)}{\mathrm{Re}} \nabla \vec{u}\right] + C\hat{k}/\mathrm{Fr}^2, \tag{6}$$

where all variables are now dimensionless, $\hat{k}$ is a unit vector parallel to the direction of gravity, $\lambda = \mu_d/\mu_c$ is the viscosity ratio, and we have two nondimensional numbers,

$$\mathrm{Re} = \frac{d u_m \rho_c}{\mu_c}, \quad \mathrm{Fr}^2 = \frac{u_m^2 \rho_c}{dg(\rho_d - \rho_c)}, \tag{7}$$

with g being the magnitude of $\vec{g}$. The Reynolds number, Re, characterizes the ratio of inertial to viscous forces and will typically be of order one. The Froude number, Fr, is the ratio of inertial to gravitational forces and is usually large $[O(100)]$ in microcapillaries, and gravitational forces are thus negligible. For simplicity, we proceed to set $\rho_d = \rho_c$ and so $\mathrm{Fr} \to \infty$, which allows the flow to remain symmetric about the axis of the tube. The boundary conditions are similarly transformed and become

$$\hat{\tau} \cdot [\lambda\{\nabla \vec{u}_d + (\nabla \vec{u}_d)^T\} - \{\nabla \vec{u}_c + (\nabla \vec{u}_c)^T\}] \cdot \hat{n} = 0 \tag{8}$$

$$\hat{n} \cdot [\{-P_d \bar{\bar{I}} + \lambda[\nabla \vec{u}_d + (\nabla \vec{u}_d)^T]\} - \{-P_c \bar{\bar{I}} + [\nabla \vec{u}_c + (\nabla \vec{u}_c)^T]\}] \cdot \hat{n} = -\frac{2}{\mathrm{Ca}} \kappa_m, \tag{9}$$

where we introduced the capillary number $\mathrm{Ca} = u_m \mu_c / \sigma$, which describes the ratio of viscous to surface forces.

III. ANALYTICAL COMPUTATION OF LIMITING CASE

We begin by presenting an analytical computation in the limiting case of negligible inertia, $\mathrm{Re} \ll 1$, for a spherical drop of radius ad, with $a \ll 1$, moving in a cylindrical tube of diameter d. Fluid in the tube is moving under a constant pressure gradient so that the flow away from the drop is parabolic with maximal velocity u_m. The governing equations then reduce to the Stokes and continuity equations,

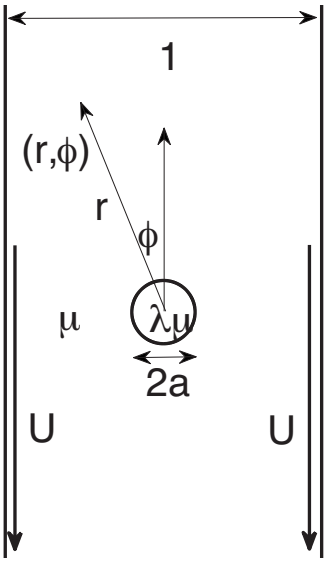

FIG. 1. Schematics of the system considered in our analytical treatment. A spherical drop of radius a and viscosity $\lambda\mu$ lies in a cylindrical tube of diameter 1 containing a carrier fluid of viscosity μ. Our frame of reference is moving with the drop, imparting a velocity U to the walls of the cylinder.

$$\nabla P = \mu \nabla^2 \vec{u}, \quad \nabla \cdot \vec{u} = 0. \tag{10}$$

Following the approach of [16], chapters 7–3, we compute the perturbation to the parabolic velocity profile due to the presence of the drop. We assume that far away from the drop, the flow is unidirectional. In a frame of reference moving with the velocity of the drop, U, the radial, V_r^∞, and tangential, V_ϕ^∞, components of the flow at infinity are, in spherical coordinates,

$$V_r^\infty = \cos\phi[(1 - U - r^2) + r^2 \cos^2\phi],$$

$$V_\phi^\infty = -\sin\phi[(1 - U - r^2) + r^2 \cos^2\phi], \tag{11}$$

where r is the distance from the center of the drop and ϕ is the angle from the vertical (Fig. 1).

We introduce perturbations to the velocity field of the drop, V^d, and carrier fluid, V^c, with radial and tangential components indexed by r and ϕ, respectively. The flow in the drop is then given by $W^d = V^d + V^\infty$ and that outside the drop by $W^c = V^c + V^\infty$. We impose the following boundary conditions at $r=a$

$$V_r^d = V_r^c = -V_r^\infty, \tag{12}$$

$$V_\phi^d = V_\phi^c, \tag{13}$$

$$\lambda\left[\frac{a}{2}\frac{\partial}{\partial r}\left(\frac{V_\phi^d}{r}\right)+\frac{1}{2a}\frac{\partial V_r^d}{\partial \phi}\right]=\frac{a}{2}\frac{\partial}{\partial r}\left(\frac{V_\phi^c}{r}\right)+\frac{1}{2a}\frac{\partial V_r^c}{\partial \phi}. \quad (14)$$

Equation (12) ensures that the drop moves with a constant velocity U and remains spherical. Equation (13) indicates that the tangential velocity must be continuous on the surface of the drop and Eq. (14) ensures that tangential stresses are also continuous on the drop surface. In addition, we require that the outer velocity field decays as $r\to\infty$ and that the inner velocity remains finite. Note that the no-slip boundary condition on the tube walls is not directly imposed and is only approximately satisfied as the perturbation velocity decreases away from the drop.

Given those conditions, the drop and carrier velocities have the general form [16]

$$V_r^c=\cos\phi\left[\frac{A}{r}-\frac{2B}{r^3}+\frac{C}{5r^3}(5\cos^2\phi-3)-\frac{2D}{r^5}(5\cos^2\phi-3)\right], \quad (15)$$

$$V_\phi^c=\sin\phi\left[-\frac{A}{2r}-\frac{B}{r^3}+\frac{C}{60r^3}(15\cos^2\phi-3)-\frac{D}{2r^5}(15\cos^2\phi-3)\right], \quad (16)$$

$$V_r^d=\cos\phi\left[\frac{Fr^4}{3}(5\cos^2\phi-3)+6Er^2(5\cos^2\phi-3)+\frac{Gr^2}{5}+2H\right], \quad (17)$$

$$V_\phi^d=\sin\phi\left[\frac{-Fr^4}{6}(15\cos^2\phi-3)-2Er^2(15\cos^2\phi-3)-\frac{2Gr^2}{5}-2H\right], \quad (18)$$

where the constants $A,B\cdots H$ can be determined by solving (using MATHEMATICA) a set of linear equations derived from the matching conditions (12)–(14). The force exerted by the fluid on the drop is then found to be $F_D=-4\pi u_m\mu_c\nabla(Ar\cos\phi)$, and we find

$$A=a(-1+U+2a^2/5)\frac{(2+3\lambda)}{2(1+\lambda)}.$$

In the absence of external forcing such as gravity, the drag F_D, and therefore the constant A, is zero and the velocity of the drop is then $U=1-\frac{2a^2}{5}$. More generally, we write the velocity of the drop as the sum of its free-stream velocity and of a small perturbation: $U=1-\frac{2a^2}{5}-\epsilon a^2$. In most application $\epsilon\ll 1$ as gravitational effects are usually negligible for liquid drops in a liquid carrier fluid. This new notation simplifies the expressions obtained for $A,B\cdots H$ to

$$A=-\frac{\epsilon a^3(2+3\lambda)}{2(1+\lambda)},\quad B=-\frac{\epsilon a^5\lambda}{4(1+\lambda)}, \quad (19)$$

$$C=\frac{-3a^5(10+11\lambda)}{14(1+\lambda)},\quad D=-\frac{a^7(16+19\lambda)}{140(1+\lambda)}, \quad (20)$$

$$E=-\frac{(11+10\lambda)}{140(1+\lambda)},\quad F=\frac{3(19+16\lambda)}{70a^2(1+\lambda)}, \quad (21)$$

$$G=\frac{5\epsilon}{2(1+\lambda)},\quad H=-\frac{\epsilon a^2(3+2\lambda)}{4(1+\lambda)}. \quad (22)$$

Note that A, B, G, and H are zero in the absence of external forcing.

We now focus on the velocity at the surface of the drop. The tangential velocity at $r=a$ is $W_\phi^d|_{r=a}=V_\phi^d+V_\phi^\infty$. From the constants given above, we have that

$$W_\phi^d|_{r=a}=\frac{a^2\sin\phi}{140(1+\lambda)}[3(25+24\lambda)-5(19+16\lambda)\cos^2\phi-70\epsilon]. \quad (23)$$

To characterize the flow inside the drop, we examine the location of stagnation points on the surface of the drop, where $W_\phi^d|_{r=a}=0$. In addition to the stagnation points at the very front and back of the drop, stagnation points occur when

$$\cos^2\phi=\frac{3(25+24\lambda)-70\epsilon}{5(19+16\lambda)}.$$

Provided ϵ satisfies $-(20+8\lambda)\le 70\epsilon\le(75+72\lambda)$, there are two stagnation points in each of the upper and lower halves of the drop. This implies the presence of three counter-rotating toroidal eddies within the drop. In the frame of reference of the drop, the central and largest portion of the drop rotates with the surface of the drop moving in the same direction as the walls. The front and back regions are rotating in the opposite direction, and a corresponding eddy is present in the carrier fluid, as can be seen on Fig. 2. We note that for matched viscosities, $\lambda=1$, a countercurrent is set up in the carrier fluid whenever the centerline fluid travels faster than the drop. The stagnation points disappear at $\epsilon=-2/5$, which corresponds to the case where the drop moves with the maximum velocity of the unperturbed flow in the pipe.

We note that force-free drops, $\epsilon=0$, have two stagnation points for all values of λ. As λ increases, the position of the stagnation points moves slightly closer to the symmetry axis, but to a remarkably small degree, with $\cos^2\phi=15/19$ ($\phi=0.48,2.66$) for $\lambda=0$, corresponding to bubbles, and $\cos^2\phi=9/10$ ($\phi=0.32,2.82$) for $\lambda=\infty$, corresponding to inviscid drops in very viscous carriers.

The presence of three toroidal rings instead of the single ring described in early studies [2] has consequences for the design of mixing devices, as we shall see in Sec. V. While only one separatrix, dividing the upper and lower parts of the drops, was initially thought to be present, we find here that there are two additional separatrices, which have to be perturbed if total mixing is to be achieved. We now proceed to investigate how the behavior observed in negligibly small drops at Re=0 is modified for drops of radii comparable to that of the tube, and when inertial effects are not negligible.

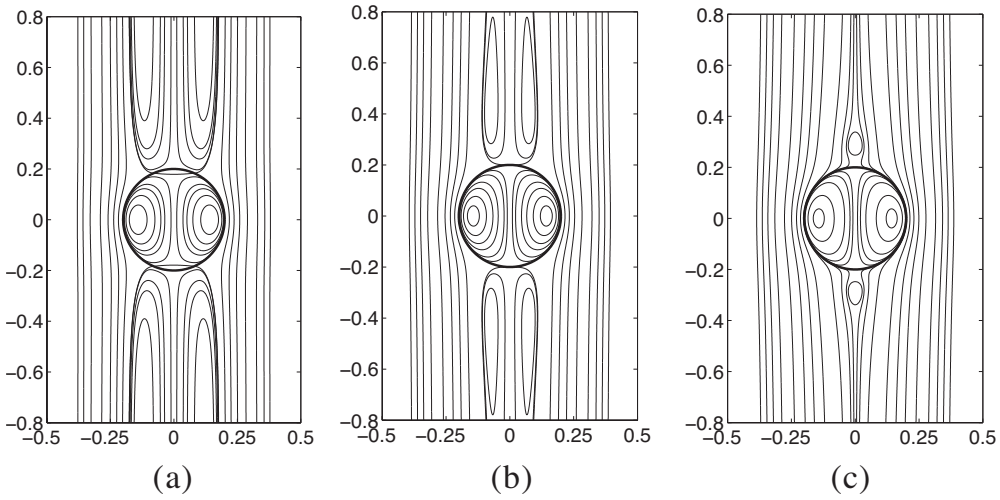

FIG. 2. Streamlines inside and outside a drop in a capillary. Here, $a=0.2$, $\lambda=\mu_d/\mu_c=1$, and $\rho_d/\rho_c=1$ in all cases and the force acting on the drop is (a) $\epsilon=0$, (b) $\epsilon=-2/5$ (drop moves at maximum velocity of unperturbed pipe flow), and (c) $\epsilon=-4/5$.

IV. NUMERICAL SIMULATIONS

A. Methodology

We performed numerical simulations of equations (5) and (6) using finite differences on a fixed staggered cartesian grid to calculate the velocity, stresses and pressure. The advection term is computed via an upwinding scheme while the diffusive term is obtained via central differences. The pressure is found via a projection method [18].

To incorporate the boundary conditions (8) and (9), we introduced a local forcing term, F_s, on the interface [15,19]. This term is of the form, in dimensional terms, $\vec{F}_s = 2\kappa_m \sigma \hat{n} \delta_S$, where δ_S is a surface delta function, which is nonzero on the interface only. Adding this forcing term to the right side of equation (6) is equivalent to enforcing the boundary conditions (8) and (9), but is much more efficient computationally. In nondimensional form, we find

$$\vec{F}_s = \frac{2}{\mathrm{We}} \kappa_m \hat{n} \delta_S, \tag{24}$$

where We is the Weber number defined as $\mathrm{We}=\rho_c u_m^2 d\sigma = \mathrm{Ca\,Re}$.

The interface is assumed to move with the fluid, $\frac{\partial S}{\partial t}=\vec{u}$, where S is the interface position, and is tracked by following markers placed in the flow. The velocity of the markers is determined by a bilinear interpolation of the velocity of the surrounding nodes. The position of the markers is then advanced in time using Euler's method. Cubic spline interpolation between those markers ensures that the interface is smooth and its curvature is well defined. The average surface forcing term per grid cell is then estimated by integrating $\vec{F}_s$ along the interface in every grid cell traversed by the interface. First-order corrections are included near the interface to take into account the discontinuity of the pressure across the interface [17].

To simulate a train of drops, similar to those generated experimentally, periodic boundary conditions are imposed in the streamwise direction (y coordinate) on all variables, with the exception of the pressure, which is then of the form $P = Ky + \tilde{P}$, with $\tilde{P}$ periodic in the y direction. Simulations are initiated with a spherical or ellipsoid-shaped drop and are run until a steady state is achieved, where both the drop shape and the flow in and around it do not change in time. To visualize the flow, passive tracers are introduced into the steady flow and tracked in time to generate streamlines as seen in the frame of reference of the drop. We simulated extensively both two-dimensional and axisymmetric cylindrical tubes, with no-slip boundary conditions at the walls. Details and validation of simulations based on the same method, though not periodic, were presented elsewhere [14] and are not repeated here.

B. Results

We first focus on the streamlines generated at steady state by a periodic array of droplets in an axisymmetric cylindrical tube. We concentrate on droplets that are only mildly deformed by viscous stresses, and therefore are not subject to break up, by fixing the Weber number at $\mathrm{We}=0.02$. The effects of increasing the Reynolds number of the pipe flow are shown in Fig. 3. We first note that for small Reynolds number, $\mathrm{Re}\leq 1$, our numerical results are in good agreement with the theoretical flow profile obtained in the limit of vanishing Reynolds number, despite the nonzero radius of the drop and the finite extent of the periodic region (four tube diameters). Even for such a small Weber number, the drop is not exactly spherical, the maximum width being reached slightly downstream of the streamwise center position. Although the front and back toroidal rings are too small and stagnant to be clearly displayed by following tracers particles, the flow in the outer fluid clearly indicates that such rings are present. For $\mathrm{Re}=0.1$, we estimate the position of the stagnation point to $\theta_s=0.43\pm0.02$ at the front and $\theta_s=0.36\pm0.02$ at the back, compared to a theoretical value of $\theta_s=0.41$. However, as the Reynolds number is increased further, the countercurrent present in the center of the tube recedes away from the drop, and the front and back toroidal rings shrink. Stag-

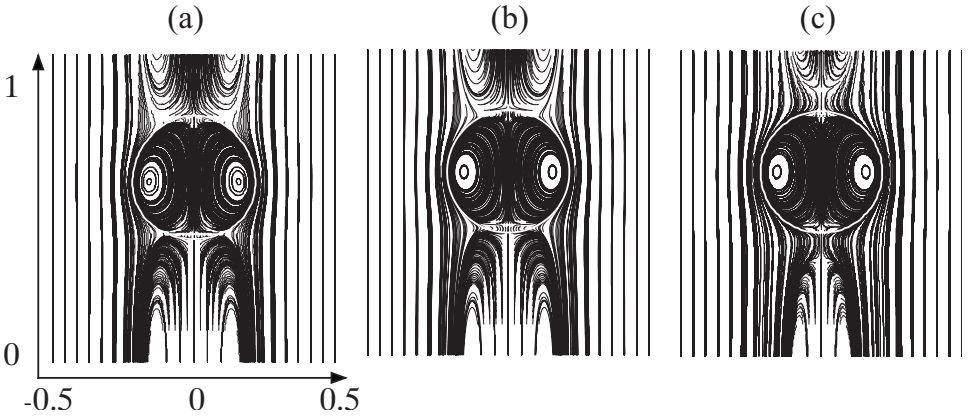

FIG. 3. Streamlines at Re=0.1 (a), 1 (b), and 10 (c) for We=0.02, $\lambda=1$, and $\rho_d/\rho_c=1$. The drop interface is shown in white, and streamlines are calculated in the frame of reference of the drop. The upper portion of the drop is its front, the lower portion is its back.

nation points, therefore, develop in the carrier fluid, both ahead and behind the drop, and the streamlines inside the drop form a single toroidal ring extending across the entire drop, the transition from one to three rings taking place near Re=3.

Next, we examine the effects of increasing the drop size so that the drop radius becomes comparable to that of the tube. As one might expect, since larger drops block a larger fraction of the tube, the countercurrent formed in the tube is extended to a broader region as the drop radius increases, see Fig. 4. The front and back toroidal rings inside the drop are correspondingly enlarged as the drop radius increases, with an approximate location of the stagnation points given by $\theta_s=0.49\pm0.02$ for drop radius $a=0.2$, $\theta_s=0.55\pm0.02$ for $a=0.3$, and $\theta_s=0.69\pm0.015$ for $a=0.4$, respectively. The rotation velocity in the front and back regions of drops of radius $a=0.2$ and 0.3 is much smaller than that in the central region, and fluid there is nearly stagnant. However, larger drops have comparable rotational velocities over their entire area.

Drops that are too large to remain spherical also exhibit such recirculating rings, which are confined to the front and back of the drop, and extend only minimally into their elongated body. Drops of even size larger are further elongated, and exhibit structure nearly identical to those of smaller drops at the front and back, and a stretched central region. For all the Reynolds numbers considered ($0.1\leq \mathrm{Re}\leq 20$), the presence of a stagnation point within the outer fluid reported at higher Reynolds numbers for smaller drops was never observed for drops of radius $a=0.3$ or larger. We note that larger drops are not front-back symmetric, a consequence of the relative high (low) pressure that forms at the front (back) of the drop.

We also investigated the effect of changes in the viscosity ratio of the drop to carrier fluid $\lambda=\mu_d/\mu_c$. Most of the features of the flow appear nearly independent of the viscosity ratio. This is consistent with the theoretical description of the tangential velocity on the drop surface, which changes only by some 15% as λ is varied. The most significant change was a slight increase in the size of the front and back toroidal regions as the drop viscosity is increased. This is presumably due to the fact that abrupt velocity variations over small length scales inside the drop are hindered as the drop viscosity increases. However, this effect remained small and for all practical purposes, the viscosity ratio had no impact of the flow profile.

V. MIXING

We study the mixing taking place in drops that are forced through sinusoidal channels by using a simplified model that

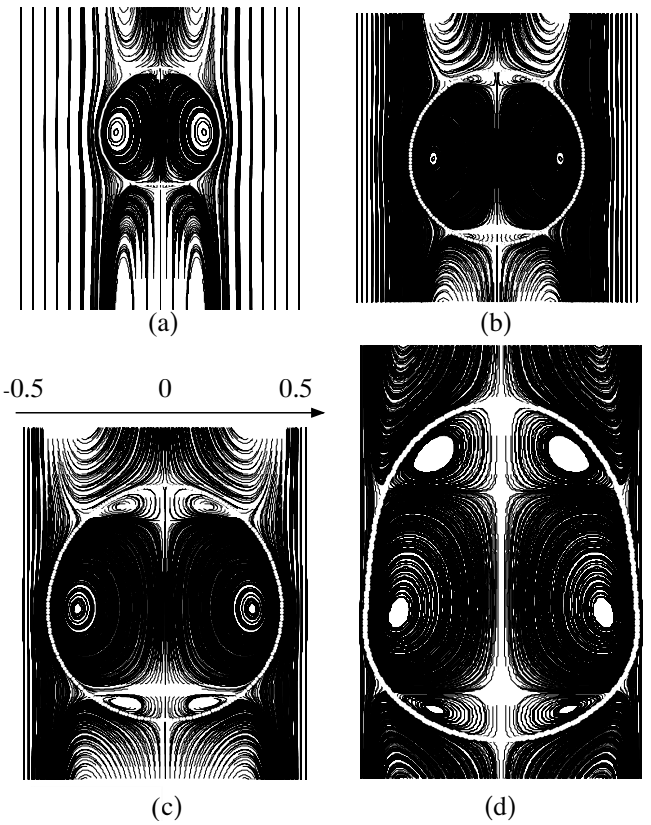

FIG. 4. Streamlines for drop radii (a) $a=0.2$, (b) 0.3, and (c) 0.4, and for a drop larger that the tube diameter for Re=1, We=0.02, $\lambda=1$, and $\rho_d/\rho_c=1$. The drop interface is shown in white, and streamlines are calculated in the frame of reference of the drop. The upper portion of the drop is its front, the lower portion is its back.

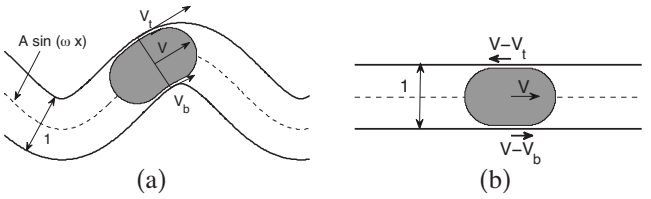

FIG. 5. Schematics of the sinusoidal tube we model with V, V_t, and V_b indicating the velocity of the tip of the drop, and the closest points on the top and bottom walls, respectively. A shear is imposed on the corresponding straight-channel, with the top wall moving with velocity $V-V_t$ and the bottom with velocity $V-V_b$.

allows simulations to be performed in a cartesian coordinate system. The channel we model is a two-dimensional sinusoidal channel (no rotational symmetry), with centerline given by $f(x)=A$ sin ωx, with x as the horizontal coordinate, and constant width 1, see Fig. 5. We choose to impose $A\omega=1$ and $\omega=1.6$ to obtain efficient mixing per arclength of the central curve, while maintaining smooth side walls (without any angles). To mimic the effect of the drop moving in a curved channel, we use a straight channel where the walls are moving with spatially uniform but time-dependent velocity, thereby imposing a time-dependent shear on the drop [9]. The wall velocity is chosen so that the center of the drop travels the same distance relative to a material point on the wall as it would in a sinusoidal channel. More precisely, if we consider a line segment spanning the width of the channel traveling with center velocity V with its tips always in contact with the side walls, see Fig. 5, the imposed straight channel, wall velocity is $V-V_t$ at the top and $V-V_b$ at the bottom, with V_t and V_b the velocity of the segment's top and bottom ends in the sinusoidal channel, respectively. The length of the periodic domain in simulations is chosen to match the arclength of a period of the sinusoidal channel. While this model does not account for the inertia of the fluid as it encounters curves in the sinusoidal channel, this effect is not expected to be significant in the low-Reynolds number regime we consider. To mimic typical experiments [2], we simulate drops that are too large to remain spherical and that are therefore elongated by the presence of the capillary's walls.

We show in Fig. 6 the position of passive tracers as an elongated drop undergoes periodic shearing, each figure corresponding to a full period. It is apparent that only three or four periods are required to achieve good mixing when the fluids to be mixed are initially segregated in the crosswise direction. The periodic shearing shifts the dividing centerline crosswise, ensuring that particles initially confined to one half of the drop may be transported in the other half.

Figures 7 and 8 show the corresponding mixing that occurs when the initial separation is in the streamwise direction. Note that in a straight channel, the white and black dots would remain separated owing to the presence of the front and back torii. The mixing in the streamwise direction is seen to be less efficient than in the crosswise direction, with a much larger concentration of black particles in the region where they were initially introduced even after five full periods. This should not come as a surprise, as the periodic shearing is designed to enhance crosswise mixing. However, despite the limitations of this design, one clearly observes cross contamination of black and white regions, showing that streamwise mixing still takes place to a significant degree.

Owing to the computational effort required to investigate the mixing within drops, we have only performed a partial study of the impact of other governing parameters. We first report that over the range of viscosity ratio we simulated, $0.2 \leq \lambda \leq 5$, no significant changes to the mixing pattern were observed when other parameters were kept constant. This is consistent with the weak influence of λ seen in the theoretical solution of Sec. III. Our simulations also revealed that the Capillary number $\mathrm{Ca}=u_m\mu_c/\sigma$ is determinant to the mixing in serpentine channels. In particular, keeping Ca fixed at $\mathrm{Ca}=0.02$ and changing the Reynolds number was found to have virtually no effect over the range $0.2 \leq \mathrm{Re} \leq 10$. However, increasing the capillary number to $\mathrm{Ca}=0.1$ results in significant drop deformation as the viscous stresses are then able to stretch the drop further. Note that these observations are consistent with the more complete description of the dependence of the drop shape on the Capillary number previously reported in [12]. As a result, the drop does not extend as close to the sides of the tube and thus does not feel the effects of the time varying shear as strongly. Consequently, the mixing is much reduced. Similarly, reducing the capillary

FIG. 6. Evolution of passive tracers for a drop forced in a sinusoidal channel simulated by time varying shearing. Each figure is a snapshot taken after one full period of the imposed shear. The governing parameters here are $\mathrm{Re}=1$, $\mathrm{Ca}=\mathrm{Re}/\mathrm{We}=0.02$, $\lambda=1$, and $\rho_c/\rho_d=1$. The upper portion of the drop is its front, the lower portion is its back.

FIG. 7. Evolution of passive tracers for a drop forced in a sinusoidal channel simulated by time varying shearing. Each figure is a snapshot taken after one full period of the imposed shear. The governing parameters here are Re=1, Ca=0.02, $\lambda=1$, and $\rho_c/\rho_d=1$. Note that in a straight channel, the black and white dots would remain separated as the black dots are initially confined to the back recirculating ring. The upper portion of the drop is its front, the lower portion is its back.

number to Ca=0.004 yields a drop that extends over nearly the entire width of the tube and thus fully feels the time varying shear, which results in faster mixing, as shown in Fig. 9. Experimentally, this is likely to be a difficult regime to maintain without having the drop wetting the walls. We thus infer that mixing is likely to be optimal for the smallest achievable Capillary number and is relatively insensitive to varying Reynolds numbers or viscosity ratios.

VI. CONCLUSION

Through our simulations of drops flowing in capillaries, we found that geometric constraints lead to the presence of three recirculating rings within a drop. When a drop is only subject to hydrodynamic forces, its speed is less than that of the fluid in the center of the tube. Our analytical investigation shows that this results in fluid catching up with the drop from behind, and moving away from its front, which leads, in a gearlike fashion, to the creation of the front and back recirculating rings. For small drops, inertial effects tend to reduce this effect and eventually (Re>3) the stationary point moves away from the drop and into the carrier fluid. On the other hand, as the drop size increases relative to that of the tube, the front and back rings grow in relative size and are seen to remain present even at higher-Reynolds numbers.

These different recirculating regions complicate the mixing picture by creating more barriers to overcome to achieve good total mixing. Mixing processes such as the serpentine channel that are designed to favor crosswise mixing are able to overcome those barriers, but only partially, leading to better crosswise than streamwise mixing. For large drops relative to the tube for which surface forces dominate viscous ones, the most determinant parameter in the mixing efficiency of these devices is the Capillary number: lower values of Ca lead to wider drops that feel more deeply the effects of changes on the tube walls and are thus better mixed. Other parameters such as the Reynolds number and the viscosity ratio have only a weak influence on the mixing process.

The picture presented here was derived for axisymmetric or two-dimensional capillaries. The presence of corners in a tube of square cross-section may affect the dynamics by facilitating the transport of fluid from on side of the drop to the other [20]. Because of the manner by which they are fabricated, most microchannels have at least two sharp corners.

FIG. 8. Evolution of passive tracers for a drop forced in a sinusoidal channel simulated by time varying shearing. Each figure is a snapshot taken after one full period of the imposed shear. The governing parameters here are Re=1, Ca=0.02, $\lambda=1$, and $\rho_c/\rho_d=1$. Note that in a straight channel, the black and white dots would remain separated as the black dots are initially confined to the front recirculating ring. The upper portion of the drop is its front, the lower portion is its back.

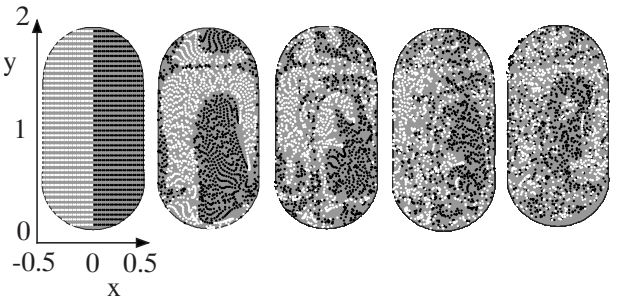

FIG. 9. Evolution of passive tracers for a drop forced in a sinusoidal channel simulated by time varying shearing. Each figure is a snapshot taken after one full period of the imposed shear. The governing parameters here are Re=1, Ca=0.004, $\lambda=1$, and $\rho_c/\rho_d=1$. The mixing pattern is similar to that for Ca=0.02 but evolves faster. The upper portion of the drop is its front; the lower portion is its back.

We obtained preliminary results using volume of fluid (VOF) simulations that indicate that the streamlines within the drop are only weakly affected by such a change in geometry. In particular, the front and back rings are expected to remain present, as the geometric constraints leading to their presence are applicable even if corners are present. We therefore expect that regardless of the cross-section shape of the tube, mixing in the streamwise direction will be hindered by the presence of the three toroidal rings. However, a more detailed picture of the effects of corners on mixing has yet to be achieved and ought to be the subject of future work.

Another effect that may be used to enhance mixing within a drop is the presence of surface tension gradient, which may be present when reagents are mixed, or may be intentionally introduced when forming the drop. As the tangential motion induced by such gradients are governed by the position of the interface rather than that of the tube, it may be possible to combine geometric effects with tangential flows to achieve even better mixing. This is the subject of ongoing research and is a promising avenue for future designs aiming at accomplishing faster and more complete mixing.

ACKNOWLEDGMENTS

The author would like to thank the James Frank institute for hosting him during the early stages of this research, as well as Wendy W. Zhang and Rustem F. Ismagilov for very constructive talks. The author was supported by NSF under Grant No. DMS Applied Mathematics 0808129.

[1] D. R. Reyes, D. Iossifidis, P. A. Auroux, and A. Manz, Anal. Chem. **74**, 2623 (2002).
[2] H. Song and R. F. Ismagilov, J. Am. Chem. Soc. **125**, 14613 (2003).
[3] N.-T. Nguyen and Z. Wu, J. Micromech. Microeng. **15**, R1 (2005).
[4] R. O. Grigoriev, Phys. Fluids **17**, 033601 (2005).
[5] H. Song, J. D. Tice, and R. F. Ismagilov, Angew. Chem., Int. Ed. **42**, 768 (2003).
[6] M. Srisa-Art, A. J. de Mello, and J. B. Edel, Phys. Rev. Lett. **101**, 014502 (2008).
[7] F. Sarrazin, K. Loubière, L. Prat, and C. Gourdon, AIChE J. **52**, 4061 (2006).
[8] B. E. Ghidersa, M. Wörner, and D. G. Cacuci, Chem. Eng. J. **101**, 285 (2004).
[9] M. Muradoglu and H. A. Stone, Phys. Fluids **17**, 073305 (2005).
[10] Z. B. Stone and H. A. Stone, Phys. Fluids **17**, 063103 (2005).
[11] N. D. Raimondi, L. Prat, C. Gourdon, and P. Cognet, Chem. Eng. Sci. **63**, 5522 (2008).
[12] F. Sarrazin, T. Bonometti, L. Prat, C. Gourdon, and J. Magnaudet, Microfluid. Nanofluid. **5**, 131 (2008).
[13] M. Wörner, B. E. Ghidersa, M. Ilic, and D. G. Cacuci, *Volume-of-Fluid Method Based Numerical Simulations of Gas-Liquid Two-Phase Flow in Confined Geometries* (Houille Blanche—Revue Internationale de l'Eau, Paris, France, 2005), Vol. 6, pp. 91–104.
[14] F. Blanchette and T. P. Bigioni, J. Fluid Mech. **620**, 333 (2009).
[15] J. U. Brackbill, D. B. Kothe, and C. Zemach, J. Comput. Phys. **100**, 335 (1992).
[16] J. Happel and H. Brenner, *Low Reynolds Number Hydrodynamics: With Special Applications to Particulate Media*, 1st ed. (Springer, New York, 1973).
[17] S. Popinet and S. Zaleski, Int. J. Numer. Methods Fluids **30**, 775 (1999).
[18] D. L. Brown, R. Cortez, and M. L. Minion, J. Comput. Phys. **168**, 464 (2001).
[19] B. Lafaurie, C. Nardone, R. Scardovelli, S. Zaleski, and G. Zanetti, J. Comput. Phys. **113**, 134 (1994).
[20] M. Dong and I. Chatzis, J. Colloid Interface Sci. **172**, 278 (1995).